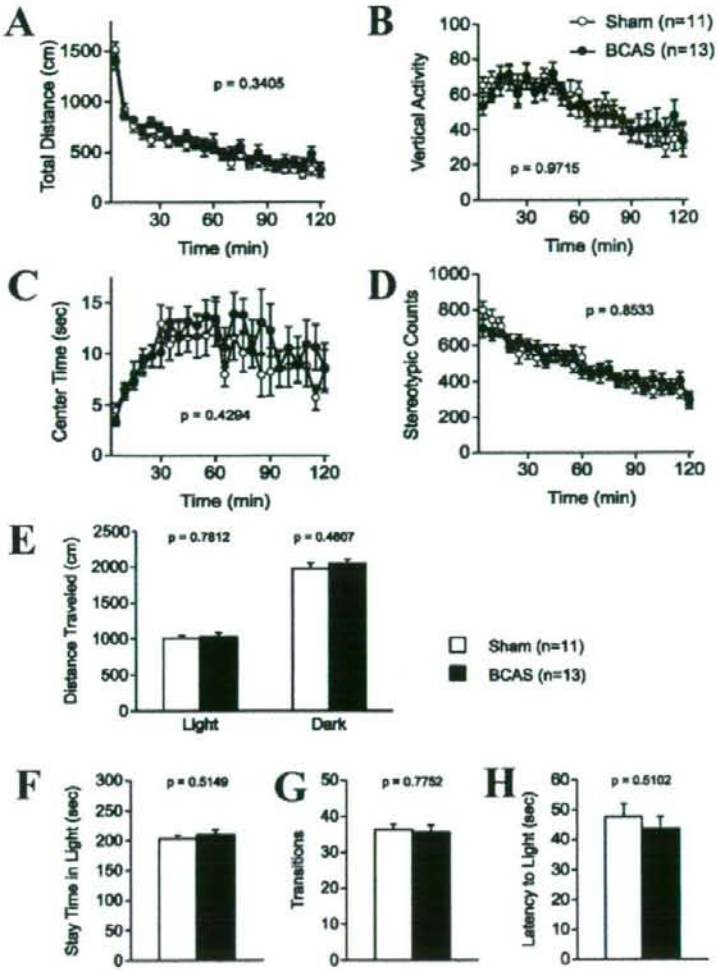

Figure 2. Locomotor activity of the control and BCAS mice in an open field test (A through D). No differences was observed for total distance traveled (group effect, $F_{1,22}=0.949$, $P=0.3405$; A), vertical activity (group effect, $F_{1,22}=0.001$, $P=0.9715$; B), time spent in the center area (group effect, $F_{1,22}=0.648$, $P=0.4294$; C), and the number of stereotypic counts (group effect, $F_{1,22}=0.035$, $P=0.8533$; D). Locomotor activity in the light/dark transition test (E through H). No difference was observed for distance traveled in light (group effect, $F_{1,22}=0.079$, $P=0.7812$) and dark chamber (group effect, $F_{1,22}=0.564$, $P=0.4607$; E), time spent in light (group effect, $F_{1,22}=0.438$, $P=0.5149$; F), number of transitions between the light and dark sides (group effect, $F_{1,22}=0.084$, $P=0.7752$; G), and latency to enter the light side ($F_{1,22}=0.448$, $P=0.5102$; H).

In spatial working memory task of the 8-arm radial maze, all 8 arms were baited with food pellets. Mice were placed on the central platform and allowed to get all 8 pellets within 25 minutes. A trial was terminated immediately after all 8 pellets were consumed or 25 minutes had elapsed. For each trial, choices of arms, latency to get all pellets, distance traveled, number of different arms chosen within the first 8 choices, and the number of revisiting, and omission errors were automatically recorded.

In reference memory task of the 8-arm radial maze, one of the 8 arms was constantly baited by one pellet in a food well and a trial was terminated immediately after one pellet was consumed. Data acquisition, control of guillotine doors, and data analysis were performed by Image RM software (see 'Image Analysis').

Image Analysis and Statistical Analysis

The applications used for the behavioral studies (Image LD, Image OF, Image PS, Image RM, and Image FZ) were based on the public domain National Institutes of Health's Image program.[18] Statistical analysis was conducted using StatView (SAS Institute). Data were analyzed by 2-way ANOVA, or 2-way repeated measures ANOVA, unless noted otherwise. Values in the table and graphs were expressed as mean±SEM.

Results

Histological Findings

All of the mice regained consciousness within a few hours after the operation, but occasionally showed transient ptosis. None of them showed any apparent motor weakness. The CBF values (ratio to the preoperative value) was not changed significantly in the sham-operated mice, but decreased to 72.4±17.3% at day 1, 77.3±15.3% at day 7 and 83.4±13.6% at day 30 after BCAS. The blood pressure measured either at day 1, 7 and 30 days was not different between the BCAS and sham-operated mice. The staining intensity of the myelinated fibers was reduced, and the integrity of the myelin was compromised in the corpus callosum (Figure 1E and 1F), caudoputamen, internal capsule and optic tract, as reported previously.[11] The remaining fibers were disorganized and vacuoles were frequently observed in the neuropil. Atrophy was not found in the optic nerve (photo not shown), although being rarefied slightly. Of the brains examined, there were no

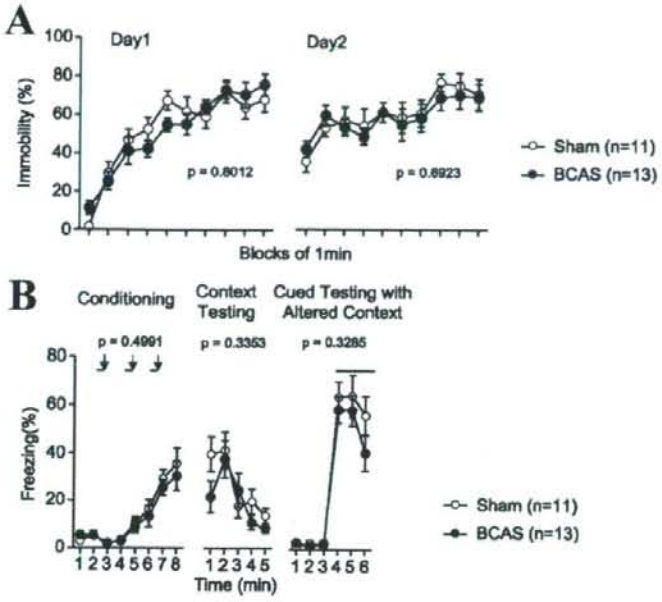

Figure 3. Behavioral despair of mice in the Porsolt forced swim test (A). Mice traveled at day 1 and day 2 (for day1, group effect, $F_{1,22}=0.065$, $P=0.8012$; for day 2, $F_{1,22}=0.161$, $P=0.6923$). Data are given as means (±SEM). Percentage of freezing during conditioning, context testing and cued testing with altered context in control and BCAS mice (B). Data are given as means (±SEM). In the contextual and cued fear conditioning test, there was no significant difference in freezing during conditioning (group effect, $F_{1,22}=0.472$, $P=0.4991$), context testing (group effect, $F_{1,22}=0.970$, $P=0.3353$), and cued testing with altered context (group effect, $F_{1,22}=0.998$, $P=0.3285$) between the groups.

infarctions or hemorrhage in any gray matter regions including the cerebral cortex, caudoputamen and hippocampus (Figure 1A through 1D, 1G, and 1H). There were only a few TUNEL positive cells in the corpus callosum (Figure 1, insets in 1E and 1F), but not in the hippocampus.

The hemispheric area was 20.4±2.7 mm^2 (mean±SEM) for BCAS mice and 20.9±1.4 mm^2 for sham-operated mice. The ventricular space area was 0.51±0.2 mm^2 for BCAS mice and 0.53±0.31 mm^2 for sham-operated mice. For both areas, there were no significant differences between the groups.

Physical Characteristics, Sensory Motor Reflexes, Nociception, Motor Coordination

As shown in the Table, there were no significant differences between BCAS and sham-operated mice in terms of their physical characteristics. Body weight in BCAS and sham-operated mice were 25.7±0.2 and 25.3±0.2, respectively, before operation, 23.8±0.2 and 24.1±0.2 after 3 days, and 27.4±0.3 and 27.0±0.4 after 30 days indicating no significant differences between the groups.

There were also no differences in sensory-motor reflexes (percent with quick response of ear twitch, normal response of whisker twitch and righting reflex, acoustic startle response), sensory-motor gating (prepulse inhibition), nociception (hot plate test), and motor coordination (wire hang and rotarod tests).

Locomotor Activity

There were also no differences between BCAS and sham-operated mice for total distance traveled, vertical activity, time spent in the center area, and the number of stereotypic counts in an open field test (Figure 2A through 2D). In the light /dark transition test (Figure 2E through 2H), there was also no differences between the groups for distance traveled in light and dark chamber, time spent in light, number of transitions between the light and dark sides and latency to enter the light side.

Porsolt Forced Swim Test, and Contextual and Cued Fear Conditioning Test

The ratio of immobility was not different between the groups both at day 1 and day 2 in Porsolt forced swim test (Figure 3A). In the contextual and cued fear conditioning test, the freezing levels during the conditioning period ($P=0.4991$), context testing ($P=0.3353$), and the cued testing with altered context ($P=0.3285$) did not differ between the groups (Figure 3B).

Learning Test

In the working memory task of the 8-arm radial maze, sham-operated mice improved their performance over training, whereas BCAS mice did not and made significantly more errors than the sham-operated control ($P<0.0001$; 2-way repeated measures ANOVA; Figure 4A). The number of different arm choices in the first 8 entries is another measure of working memory performance. The number ranged from 5.3 for a chance performance to 8 for a perfect performance. However, sham-operated mice improved significantly more than BCAS mice with each consecutive training session ($P=0.0002$, 2-way repeated measures ANOVA; Figure 4B).

On the other hand, there were no significant differences between the groups in the reference memory task of the 8-arm radial maze ($F_{1,20}=2.878$, $P=0.1053$, 2-way repeated measures ANOVA; Figure 4C). After 8-arm radial maze test, the same animals were subjected to the open field test (Figure 4D through 4G). The activity level of BCAS mice was similar to the sham-operated mice (total distance; $F_{1,19}=0.050$,

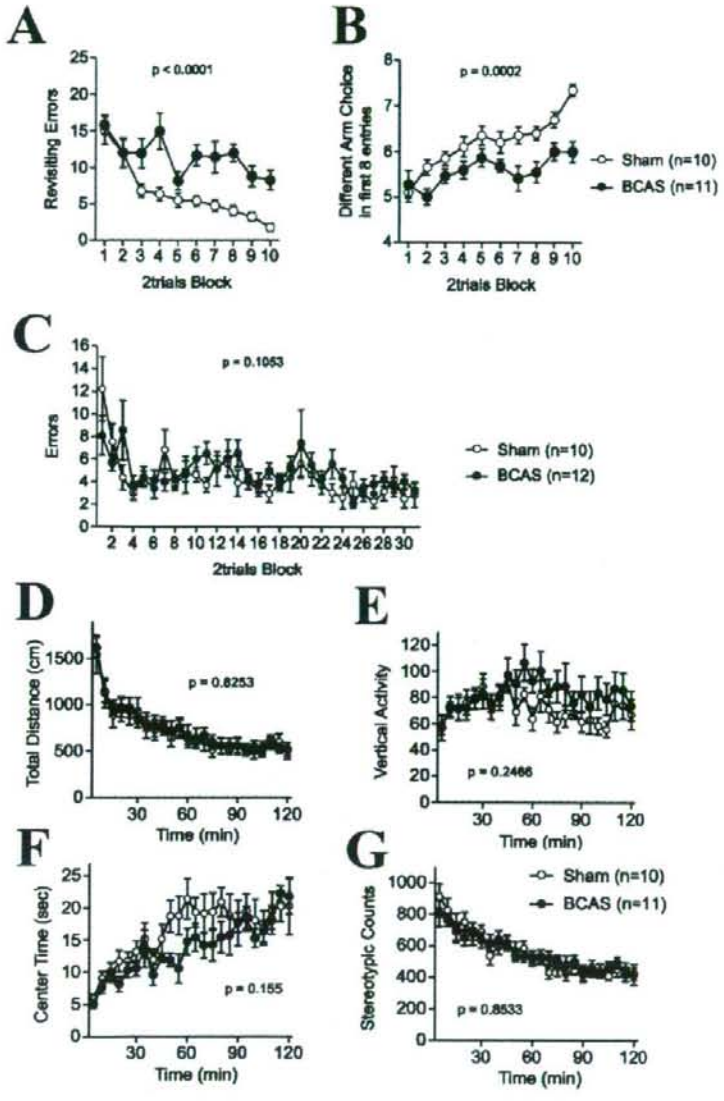

Figure 4. Working memory (A and B) and reference memory (C) of the control and BCAS mice in an 8-arm radial maze test. Data are given as means (±SEM) for revisiting errors (A), and different arm choices (B) in working memory task, and errors in reference memory task (C). BCAS mice showed a lesser number of different arm choices (group effect, $F_{1,19}=20.519$, $P=0.0002$; A), and more revisiting errors (group effect, $F_{1,19}=43.267$, $P<0.0001$; B) as compared with the control mice. There was no significant difference in the number of errors in reference memory task between the groups (group effect, $F_{1,26}=2.878$, $P=0.1053$; C). Locomotor activity of the control and BCAS mice in the open field test (D through G). No difference was observed for total distance (group effect, $F_{1,19}=0.050$, $P=0.8253$; D), vertical activity (group effect, $F_{1,19}=0.693$, $P=0.4155$; E), time spent in the center area (group effect, $F_{1,19}=2.194$, $P=0.155$; F), and the number of stereotypic counts (group effect, $F_{1,19}=0.002$, $P=0.9654$; G).

$P=0.8253$, 2-way repeated measures ANOVA). Thus, spatial reference memory required to correctly perform the reference memory task in the 8-arm radial maze does not appear to be affected in the BCAS mice.

Discussion

In the rat model of chronic cerebral hypoperfusion, although we did not find any changes in the hippocampus,[5] previous studies have reported hippocampal CA1 damages.[12,13] Hippocampal damages may cause impairment of both reference and working memory, and therefore make it difficult to determine whether the cognitive impairment was a consequence of WM lesions. Variability in hippocampal damage in the rat model may be caused by a relatively severe reduction of the CBF (30% to 50% of the preoperative values), in which low variability around the threshold may determine the occurrence of hippocampal changes.

In the current mouse model, if the degree of chronic cerebral hypoperfusion is appropriately controlled by changing the internal diameter of the microcoils, the decrease in CBF can be milder to selectively affect the cerebral WM. Using microcoils with a diameter of 0.16 mm, the CBF was decreased to 51.4±11.5% of the preoperative values with the resultant hippocampal CA1 damage.[11] However, using microcoils with a diameter of 0.18 mm or 0.20 mm, the CBF was decreased to 67.3±18.5% and 77.3±13.4%, respectively, and the histological damages including activation of microglia and astroglia were restricted to the WM.[11]

The BCAS mice showed no difference to the controls in the comprehensive behavioral tests, including a complete neurological screen, prepulse inhibition, hot plate, open field, light/dark transition, Porsolt forced swim and contextual and cued fear conditioning. Thus, this screen showed that these mice have no deficits in physical characteristics and sensory/motor functions. In addition, BCAS mice showed normal spatial reference memory in the 8-arm radial maze test. Spatial reference memory task was related to cognitive domains thought to rely on the integrity of the hippocampus, and therefore preserved reference memory is in agreement with lack of histological damage in the hippocampus. In contrast, working memory impairment may be attributable to either frontal WM lesions or hippocampal damages which are undetectable by the present methods. In previous studies, working memory deficits have been related either to the hippocampus or frontal-subcortical circuits in the rodent[14,19,20] and likely primates.[21,22] Therefore, the disruption of WM tracts especially within the prefrontal cortex may be another mechanism for age-related changes in working memory function.[23]

We successfully developed a mouse model of chronic cerebral hypoperfusion, which showed cognitive abnormalities with only a mild damage to the visual system. In the rat model, working memory and gait performances have been shown to be impaired.[12,13,24] However, the rat model exhibits severe degeneration and atrophy of the optic nerve.[5,14,25,26] The possibility cannot be ruled out that the visual system impairment may compromise the behavioral test, because visual cues contribute to discrimination even in the rodent.[27]

In this setting, the rat model is suitable for pharmacological evaluation because of prompt emergence of WM changes and easy applicability of stereotaxic surgery. In contrast, the mouse, which is readily amenable to gene knockout and manipulation and has advantages in cognitive evaluation, can be a model of subcortical vascular dementia suited for pathogenetic analysis and behavioral assessment.

Sources of Funding

This work was supported in part by a Grant-in-Aid for scientific research (C) (18590936) from the Japanese Ministry of Education, Culture, Sports, Science and Technology. This study is a part of joint research, which is focusing on the development of the basis of technology for establishing COE for nano-medicine, carried out through Kyoto City Collaboration of Regional Entities for Advancing Technology Excellence (CREATE) assigned by Japan Science and Technology Agency (JST).

Disclosures

None.

References

1. Roman GC, Erkinjuntti T, Wallin A, Pantoni L, Chui HC. Subcortical ischaemic vascular dementia. *Lancet Neurol*. 2002;1:426–436.
2. Fernando MS, Simpson JE, Matthews F, Brayne C, Lewis CE, Barber R, Kalaria RN, Forster G, Esteves F, Wharton SB, Shaw PJ, O'Brien JT, Ince PG; MRC Cognitive Function and Ageing Neuropathology Study Group. White matter lesions in an unselected cohort of the elderly: molecular pathology suggests origin from chronic hypoperfusion injury. *Stroke*. 2006;37:1391–1398.
3. Kudo T, Tada K, Takeda M, Nishimura T. Learning impairment and microtubule-associated protein 2 decrease in gerbils under chronic cerebral hypoperfusion. *Stroke*. 1990;21:1205–1209.
4. Hattori H, Takeda M, Kudo T, Nishimura T, Hashimoto S. Cumulative white matter changes in the gerbil brain under chronic cerebral hypoperfusion. *Acta Neuropathol (Berl)*. 1992;84:437–442.
5. Wakita H, Tomimoto H, Akiguchi I, Kimura J. Glial activation and white matter changes in the rat brain induced by chronic cerebral hypoperfusion: an immunohistochemical study. *Acta Neuropathol (Berl)*. 1994;87:484–492.
6. Kurumatani T, Kudo T, Ikura Y, Takeda M. White matter changes in the gerbil brain under chronic cerebral hypoperfusion. *Stroke*. 1998;29:1058–1062.
7. Tomimoto H, Ihara M, Wakita H, Ohtani R, Lin JX, Akiguchi I, Kinoshita M, Shibasaki H. Chronic cerebral hypoperfusion induces white matter lesions and loss of oligodendroglia with DNA fragmentation in the rat. *Acta Neuropathol (Berl)*. 2003;106:527–534.
8. Lin J-Xi, Tomimoto H, Akiguchi I, Wakita H, Shibasaki H, Horie R. White matter lesions and alteration of vascular cell composition in the brain of spontaneously hypertensive rats. *Neuro Report*. 2001;12:1835–1839.
9. de Groot JC, de Leeuw FE, Oudkerk M, Hofman A, Jolles J, Breteler MMB. Cerebral white matter lesions and subjective cognitive dysfunction: The Rotterdam Scan Study. *Neurology*. 2001;56:1539–1545.
10. Tullberg M, Fletcher E, DeCarli C, Mungas D, Reed BR, Harvey DJ, Weiner MW, Chui HC, Jagust WJ. White matter lesions impair frontal lobe function regardless of their location. *Neurology*. 2004;63:246–253.
11. Shibata M, Ohtani R, Ihara M, Tomimoto H. White matter lesions and glial activation in a novel mouse model of chronic cerebral hypoperfusion. *Stroke*. 2004;35:2598–2603.
12. Ni JW, Matsumoto K, Li HB, Murakami Y, Watanabe H. Neuronal damage and decrease of central acetylcholine level following permanent occlusion of bilateral common carotid arteries in rat. *Brain Res*. 1995;673:290–296.
13. Tanaka K, Ogawa N, Asanuma M, Kondo Y, Nomura M. Relationship between cholinergic dysfunction and discrimination learning disabilities in Wistar rats following chronic cerebral hypoperfusion. *Brain Res*. 1996;729:55–65.
14. Ohta H, Nishikawa H, Kimura H, Anayama H, Miyamoto M. Chronic cerebral hypoperfusion by permanent internal carotid ligation produces learning impairment without brain damage in rats. *Neuroscience*. 1997;79:1039–1050.
15. Nakaji K, Ihara M, Takahashi C, Itohara S, Noda M, Takahashi R, Tomimoto H. MMP-2 play a critical role in the pathogenesis of white matter lesions after chronic cerebral hypoperfusion in rodents. *Stroke*. 2006;37:2816–2823.
16. Crawley JN. *What's Wrong With My Mouse? Behavioral Phenotyping of Transgenic and Knockout Mice*. New York, NY: Wiley-Liss; 2000.
17. Miyakawa T, Yamada M, Duttaroy A, Wess J. Hyperactivity and intact hippocampus-dependent learning in mice lacking the M1 muscarinic acetylcholine receptor. *J Neurosci*. 2001;21:5239–5250.
18. Miyakawa T, Leiter LM, Gerber DJ, Gainetdinov RR, Sotnikova TD, Zeng H, Caron MG, Tonegawa S. Conditional calcineurin knockout mice exhibit multiple abnormal behaviors related to schizophrenia. *Proc Natl Acad Sci U S A*. 2003;100:8987–8992.
19. Hiraga Y, Iwasaki T. Recent advances in studies of rat memory in the radial-arm maze. *Yakubutsu Seishin Kodo*. 1983;3:99–108.
20. Sarti C, Pantoni L, Bartolini L, Inzitari D. Cognitive impairment and chronic cerebral hypoperfusion: what can be learned from experimental models. *J Neurol Sci*. 2002;203–204:263–266.
21. Funahashi S, Bruce CJ, Goldman-Rakic PS. Mnemonic coding of visual space in the monkey's dorsolateral prefrontal cortex. *J Neurophysiol*. 1989;61:331–349.
22. Nordahl CW, Ranganath C, Yonelinas AP, Decarli C, Fletcher E, Jagust WJ. White matter changes compromise prefrontal cortex function in healthy elderly individuals. *J Cogn Neurosci*. 2006;18:418–429.
23. Burton EJ, Kenny RA, O'Brien J, Stephens S, Bradbury M, Rowan E, Kalaria R, Firbank M, Wesnes K, Ballard C. White matter hyperintensities are associated with impairment of memory, attention, and global cognitive performance in older stroke patients. *Stroke*. 2004;35:1270–1275.
24. Sarti C, Pantoni L, Bartolini L, Inzitari D. Persistent impairment of gait performances and working memory after bilateral common carotid artery occlusion in the adult Wistar rat. *Behav Brain Res*. 2002;136:13–20.
25. Takamatsu J, Hirano A, Levy D, Henkind P. Experimental bilateral carotid artery occlusion: a study of the optic nerve in the rat. *Neuropathol Appl Neurol*. 1984;10:423–428.
26. Davidson CM Pappas BA, Stevens WD, Fortin T, Bennett SAL. Chronic cerebral hypoperfusion: loss of pupillary reflex, visual impairment and retinal neurodegeneration. *Brain Res*. 2000;859:96–103.
27. Sutherland RJ, Hamilton DA. Rodent spatial navigation: at the crossroads of cognition and movement. *Neurosci Biobehav Rev*. 2004;28:687–697.

J Neural Transm (2007) 114: 577–584
DOI 10.1007/s00702-006-0610-7
Printed in the Netherlands

Journal of Neural Transmission

Association of vascular parkinsonism with impaired neuronal integrity in the striatum

M. Ihara[1], H. Tomimoto[1], K. Ishizu[2], H. Yoshida[3], N. Sawamoto[3], K. Hashikawa[3], H. Fukuyama[3]

[1] Department of Neurology, Kyoto University Graduate School of Medicine, Kyoto, Japan
[2] Nuclear Medicine and Diagnostic Radiology, Kyoto University Graduate School of Medicine, Kyoto, Japan
[3] Human Brain Research Center, Kyoto University Graduate School of Medicine, Kyoto, Japan

Received: May 23, 2006 / Accepted: November 14, 2006 / Published online: January 18, 2007

Summary The purpose of this study is to identify the underlying differences between patients with white matter lesions (WMLs) who manifested gait disturbance suggestive of vascular parkinsonism (VaP) and those who did not, using the PET scan. Fourteen patients with extensive WMLs, as determined by MRI, were divided into two groups – 7 with gait disturbance and 7 without it. Neuronal integrity was evaluated with a PET scan using [^{11}C]flumazenil (FMZ) by calculating the distribution volume of FMZ (FMZ-V_d) in various regions of interest by non-linear curve fitting. Additionally, tracer kinetic analysis was applied for voxel-by-voxel quantification of FMZ-V_d and data analysis was performed using statistical parametric mapping. The striatal FMZ-V_d values were inversely correlated with the motor UPDRS scores ($r = 0.70$, $p < 0.005$), and their reductions were associated with the presence of gait disturbance. Therefore, differences in neuronal integrity in the striatum may determine whether patients with WMLs develop VaP or not.

Keywords: Vascular parkinsonism, flumazenil, striatum, white matter, small vessel disease

Introduction

Vascular parkinsonism (VaP) develops as a consequence of heterogeneous groups of cerebrovascular diseases (Winikates and Jankovic, 1999; Sibon et al., 2004; Ebersbach and Poewe, 2006). The incidence of VaP is reported to be 3.4% in an autopsy series of 759 patients with clinical parkinsonism (Jellinger, 2003). VaP primarily affects the lower body and is characterized by a poor response to levodopa, suggesting that it has a different pathophysiology than idiopathic Parkinson's disease (IPD) (van Zagten et al., 1998; Winikates and Jankovic, 1999; Foltynie et al., 2002; Sibon et al., 2004; Rampello et al., 2005). Although striatal lacunar infarcts have been thought to cause VaP (Zijlmans et al., 1995), a meta-analysis revealed that only 9% of patients with these lesions developed parkinsonism (Foltynie et al., 2002); one group even reported an absence of a correlation between the two conditions (Bhatia and Marsden, 1994). Furthermore, a clinicopathological study suggested that white matter lesions (WMLs) rather than striatal lacunar infarcts were the more direct cause of VaP (Yamanouchi and Nagura, 1997). Inconsistencies between these studies may have, at least partially, been due to the heterogenous features of stroke patients.

In this study, we sought to identify the underlying differences between patients with WMLs who manifested gait disturbance suggestive of VaP and those who did not, using the PET scan. Since varying degrees of WMLs and striatal lacunar infarcts are seen heterogeneously in patients with small vessel disease (Yamanouchi and Nagura, 1997), we exclusively enrolled patients who exhibited extensive WMLs in order to minimize these differences. We specifically used the central benzodiazepine receptor (BZR) ligand [^{11}C]-flumazenil (FMZ) as a PET tracer, since this ligand was reported to bind to gamma-aminobutyric acid type A ($GABA_A$) receptors that are widely expressed on cerebral neurons (Olsen, 1981) and as such, can be used to assess the integrity of neurons (Heiss et al., 1998; Ihara et al., 2001, 2004). We also examined cerebral blood flow (CBF), cerebral metabolic rate of oxygen metabolism ($CMRO_2$), and the oxygen extraction fraction (OEF) using the ^{15}O gas steady-state method.

Correspondence: Masafumi Ihara, MD, PhD, Department of Neurology, Kyoto University Graduate School of Medicine, Shogoin, Sakyo, Kyoto 606-8507, Japan
e-mail: ihara@kuhp.kyoto-u.ac.jp

Material and methods

Patients

Fourteen patients whose T2-weighted MRI scans revealed confluent hyperintensities in the subcortical white matter (Schmidt scale score of 3) (Schmidt et al. 1996), as determined at our Neurology Clinic from May 1999 to March 2005, as well as several punctate high-intensity areas in the striatum and/or thalamus were enrolled independently of their clinical status and subjected to PET scanning (Fig. 1). Each subject was fully informed about the experimental procedures and provided written, informed consent; their inclusion in this study was approved by the Ethical Committee

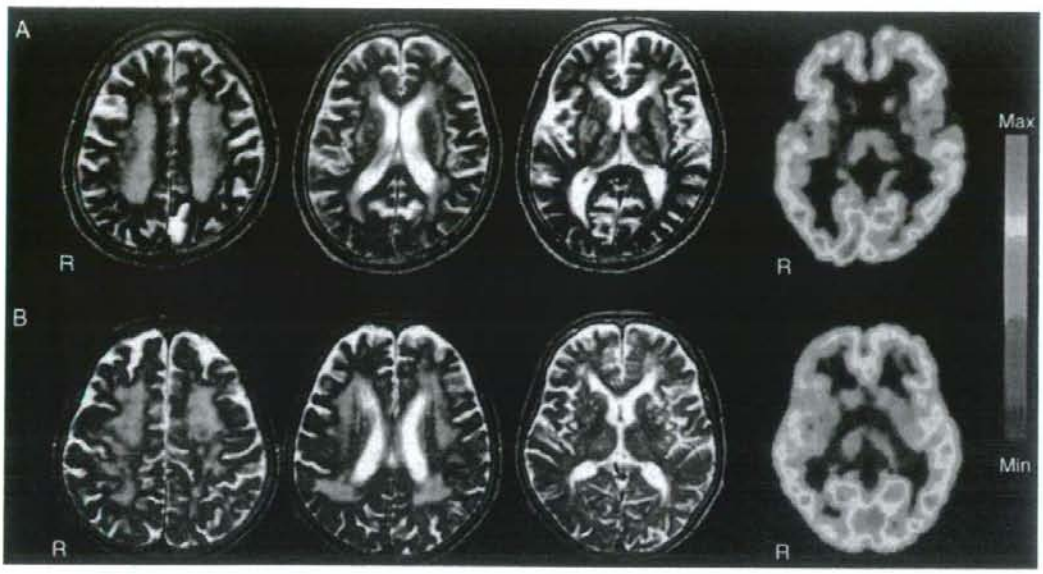

Fig. 1. Representative T2-weighted MRIs and parametric PET images of FMZ-V_d in two patients with WMLs (A, gait disturbance; B, no gait disturbance). FMZ-V_d values are noted in the pseudocolor scale ranging from 0 to 10 ml/gm. *R* indicates right

Table 1. Demographic features of the patients

Variable	Group A, WMLs with gait disturbance	Group B, WMLs without gait disturbance	*p*
No. of patients	7 (3 men, 4 women)	7 (2 men, 5 women)	
Mean age (range), y	73.7 ± 4.6 (68–80)	77.3 ± 2.7 (72–80)	0.1
No. of lacunae in the striatum	1.14 ± 0.90	0.57 ± 0.54	0.17
Area of lacunae in the striatum (mm^2)	42.8 ± 30.3	21.7 ± 21.5	0.16
Motor UPDRS (0–108)	45.4 ± 15.0	8.2 ± 9.2	<0.001
MMSE score (0–30)	21.0 ± 6.3	27.0 ± 3.9	0.05
Dysarthria, No. (%)	3 (43)	0 (0)	0.19
Pseudobulbar palsy, No. (%)	1 (14)	0 (0)	>0.99
Urinary incontinence, No. (%)	3 (43)	1 (20)	0.56
Hypertension, No. (%)	5 (71)	4 (57)	>0.99
BP control (systolic BP >140 mmHg), No. (%)	1 (14)	0 (0)	>0.99
Diabetes mellitus, No. (%)	2 (29)	0 (0)	0.46
Cigarette smoking, No. (%)	3 (43)	3 (43)	>0.99
Microalbuminuria, No. (%)	2 (29)	0 (0)	0.46
Previous cerebrovascular events, No. (%)	2 (29)	1 (14)	>0.99
Previous myocardial infarction, No. (%)	2 (29)	1 (14)	0.47
Use of antiplatelets, No. (%)	5 (71)	5 (71)	>0.99
Use of anticoagulants, No. (%)	0 (0)	2 (29)	0.46
Total cholesterol, mg/dl	223.7 ± 23.8	199.7 ± 15.3	0.27
Triglyceride, mg/dl	106.2 ± 56.1	124.0 ± 54.0	0.55
Hematocrit, %	38.1 ± 2.6	35.9 ± 2.7	0.14

Data are presented as mean ± SD. *UPDRS* Unified Parkinson's disease rating scale; *MMSE* mini-mental state examination; *BP* blood pressure.

of our facility. If a subject was not fully competent due to dementia, we obtained full informed consent from his/her proxy. None of our patients had apparent lesions in the cerebral cortex, midbrain, or hippocampus. MR angiography or duplex color-coded sonography revealed an absence of apparent stenosis (greater than 50%) in the major intracranial and extracranial vessels. None of our patients had a history of taking any sedative-hypnotic benzodiazepines within the past 3 months that could have affected their BZR assessment. All subjects underwent a general physical and neurological examination, the motor subscale ratings of the Unified Parkinson's Disease Rating Scale (UPDRS), and Mini-Mental State Examination (MMSE) in a blind fashion with respect to the MRI results. We diagnosed VaP if the patient with WMLs met all the following criteria: symmetric parkinsonian syndrome; presence of gait disorder (including wide-based, small steppage, or frozen gait) plus at least one of the following two extrapyramidal signs: rigidity and bradykinesia; exclusion of drug-induced parkinsonism; poor response to adequate dose of anti-parkinsonian agents.

Synthesis of [^{11}C]FMZ, PET scanning, and data analysis

[^{11}C] FMZ was synthesized as previously described (Magata et al., 2003). Its radiochemical purity was found to be >98.5% and its specific activity was 53.4 ± 14.7 GBq/μmol ($n = 14$).

All 14 patients were scanned with a PET scanner (Advance; General Electric, Milwaukee, MI) that was run in 2-dimensional mode (Magata et al., 2003). Arterial blood samples were drawn, and metabolite correction of [^{11}C] FMZ was performed by the plasma extraction method (Magata et al., 2003) for 12 patients and by the whole blood extraction method, which was shown to be equivalent to the plasma extraction method (Magata et al., 2003), for 2 patients. Dynamic imaging was performed using 2D acquisition mode for 50 min after injection (sequence; 6 × 30 sec, 7 × 1 min, 5 × 2 min, 6 × 5 min). Six patients with parkinsonism and five patients without parkinsonism underwent ^{15}O gas steady-state examination within two weeks of FMZ-PET to quantify their CBF and $CMRO_2$ using the above PET scanner (Ihara et al., 2004). We followed the protocol for inhalation of [^{15}O] CO_2, [^{15}O] O_2, and [^{15}O] CO as previously reported (Yamauchi et al., 1999). PET data were reconstructed into 3-dimensional images parallel to the orbitomeatal line, so that each image consisted of 64 planes with 2-mm cubic voxels. Images were displayed using PMOD software version 2.4 (PMOD Technologies Ltd., Zurich, Switzerland) (Mikolajczyk et al., 1998).

ROI-based analysis

Regions of interest (ROIs) were defined on summed FMZ uptake images by point-and-click or manual drawing mode using PMOD (Mikolajczyk et al., 1998; Ihara et al., 2004). Briefly, for cortical regions, ROIs were drawn by hand in narrow strips that overlay the cortical mantle in the following regions: frontal cortex including Brodmann area's 8, 9, 10, 44, 45 and 46, temporal cortex including areas 21, 22 and 37, parietal cortex including areas 5, 7, 39 and 40, and occipital cortex including areas 17, 18 and 19, while intracranial sulci were avoided in order to minimize the partial volume effect. We also defined ROIs in the thalamus, basal ganglia (caudatoputamen), cerebellum, and centrum semiovale. Each patient's ROIs were saved. Based on a two compartment two parameter model using metabolite-corrected arterial input and PET-measured cerebral radioactivity, the distribution volume of FMZ ($FMZ\text{-}V_d$) was calculated in the defined ROIs by non-linear curve fitting based on the Gauss-Newton method. Values in homologous regions of each hemisphere were averaged. The CO, O_2, CO_2 images were coregistered to the FMZ image (Pmod software). The ROIs drawn on the FMZ image were transferred to the gas images, and their raw radioactivity counts were measured in all ROIs. Based on the steady-state method, regional CBF, $CMRO_2$ and OEF were calculated using each ROI value (Frackowiak et al., 1980). The $CMRO_2$ and OEF were corrected for CBV (Lammertsma and Jones, 1983).

Voxel-by-voxel analysis

Using PMOD, pixel-wise calculation was performed to yield parametric images of $FMZ\text{-}V_d$ (Mikolajczyk et al., 1998; Ihara et al., 2004). Briefly, the loaded image data were first pre-processed with arterial input curve. Classic Logan plot model was then applied to the time vector in each individual pixel. The pixel-wise results were assembled into parametric images of $FMZ\text{-}V_d$. These parametric images were analyzed using SPM2 (Wellcome Department of Cognitive Neurology, London, UK) that was run on Matlab6.5 (The MathWorks, Natick, MA). The images were transformed into the standard SPM2 PET template using the early phase of the FMZ image added (0–10 min) as a blood flow image. As a final pre-processing step, the images were smoothed using a 10 mm (full width at half maximum) isotropic Gaussian kernel.

Magnetic resonance imaging

Brain MRIs were obtained using a 1.5 Tesla MR scanner (Signa Horizon; General Electric). T1-weighted axial images were obtained using a spin

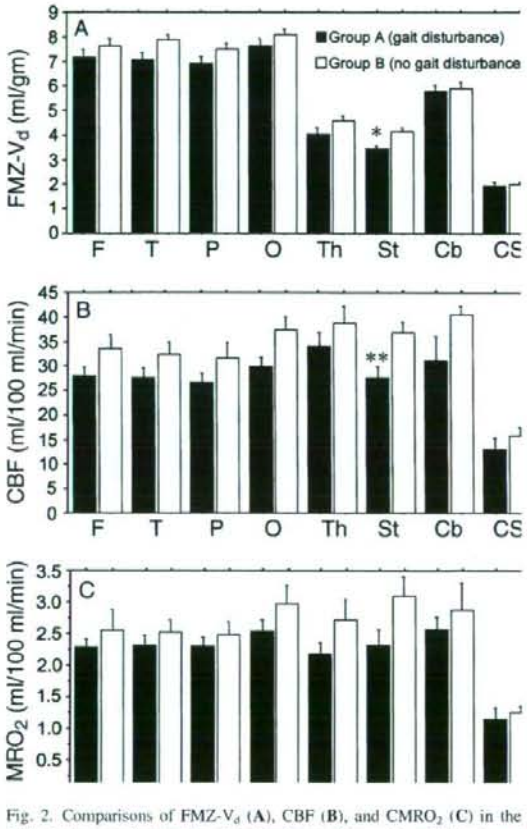

Fig. 2. Comparisons of $FMZ\text{-}V_d$ (**A**), CBF (**B**), and $CMRO_2$ (**C**) in the ROIs between patients with gait disturbance (Group A: solid bars) and those without gait disturbance (Group B: open bars). Bars represent SEM. *F* indicates frontal cortex; *T*, temporal cortex; *P*, parietal cortex; *O*, occipital cortex; *Th*, thalamus; *St*, striatum; *Cb*, cerebellum; and *CS*, centrum semiovale. $^{*}p < 0.001$; $^{**}p < 0.05$

echo pulse sequence with a repetition time of 400 msec and an echo time of 15 msec. Axial T2-weighted images were also obtained (repetition time, 3000 msec; echo time, 100 msec). Axial images were obtained in parallel to the orbitomeatal line. Slice thickness was 5 mm, with an interslice gap of 1.8 mm in the axial plane.

Lacunar infarction was defined as a hyperintensity area (5 mm ≤ diameter < 15 mm) on T2-weighted images which was seen as a low-signal intensity on T1-weighted images (Braffman et al., 1988). To reduce the risk of inclusion of enlarged perivascular spaces, lesions <5 mm were not counted as infarctions. The area of striatal lacunar infarction was approximated on a T2-weighted axial slice traversing the anterior horn of the ventricle and the thalamus (see Fig. 5) on a Macintosh PowerPC computer using the public domain NIH Image1.61 program (NIH).

The extent of cerebral atrophy was assessed by regional volumetric measures normalized for total intracranial area on three T2-weighted axial slices (see Fig. 5) using the NIH Image1.61 program. In brief, we outlined the inner boundary of the calvarium manually on T2-weighted axial images to determine the total intracranial area. The images were then binarized with intensity threshold set at 60% of mean intracranial pixel values within the outlined area. After the ventricular and subdural areas were semiautomatically outlined using the wand tool, the number of pixels in each area was divided by that in the total intracranial area to calculate normalized ventricular and subdural area. Finally, subtraction of the normalized ventricular and subdural areas from the total intracranial area (value 1.0) yielded normalized parenchymal area.

Statistical analysis

The statistical significance of intergroup differences was assessed with the Fisher's exact test for categorical variables, the Mann–Whitney *U*-test for continuous parametric variables of demographic data, and by ANOVA or ANCOVA for ROI-based analysis of FMZ-V_a, CBF, $CMRO_2$, and OEF (StatView5.0; SAS Institute, Cary, NC). Pearson correlation analysis was performed to observe possible links between the variables.

For voxel-based analysis, significant differences in FMZ-V_a between groups were estimated according to the general linear model at each and every voxel of the normalized and smoothed images (Friston et al., 1995). A linear contrast was used to test hypotheses relating to specific focal effects. The resulting set of voxel values for each contrast constituted a statistical parametric map (SPM{t}). The SPM{t} was thresholded at $P_{uncorr} < 0.001$ without multiple comparison.

Results

The demographic features of our patients were summarized in Table 1. The subjects were divided into two groups; i.e., patients with gait disturbance (so-called 'lower body' parkinsonism) suggestive of VaP (group A; $n = 7$) and those without it (group B; $n = 7$). Family history with regard to parkinsonism was unremarkable in all patients and there were no significant differences in patient age between groups ($p = 0.10$). The motor disability was measured by the motor UPDRS score; patients in group A showed significantly more severe motor disability than those in group B ($p < 0.001$). The MMSE score was reduced in the group A but with no statistical significance ($p = 0.053$).

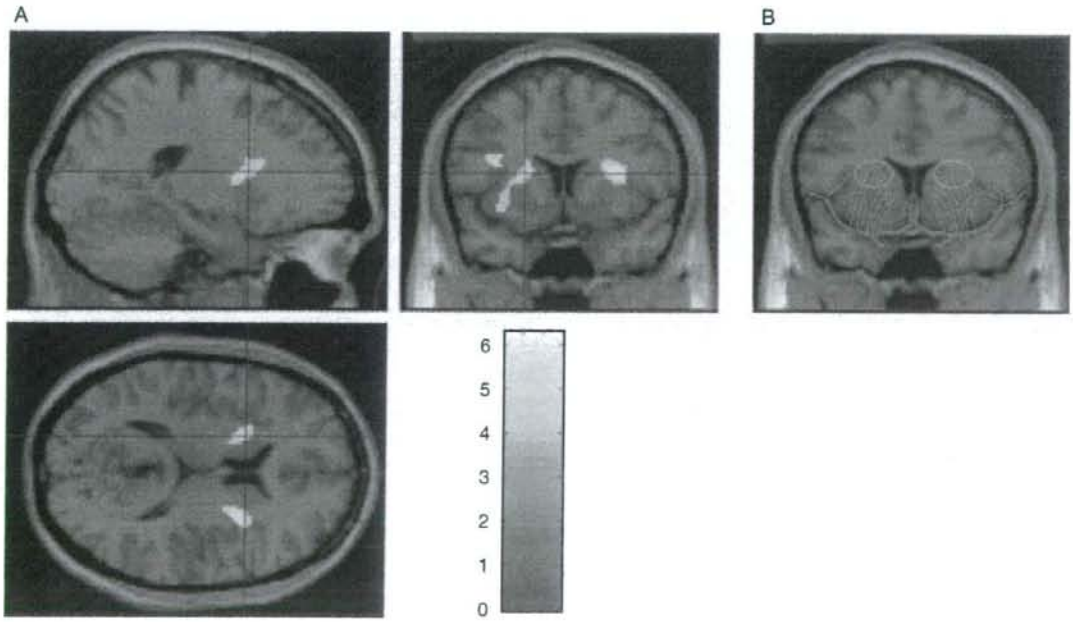

Fig. 3. Voxel-based analysis of [^{11}C]flumazenil-PET. A Statistical results were overlaid onto the brain slices of the standard MRI template of SPM2. Color scale: *t* scores (maximum $t = 6.83$, corresponding to $Z = 4.08$). *R* indicates right. B A diagram showing that FMZ-V_a is reduced in a part of the territory of lateral lenticulostriate arteries (artery, red lines; territory, dotted circles)

All patients had at least one risk factor for ischemic cerebrovascular disease which included hypertension, diabetes mellitus, hyperlipidemia, and smoking. Although there were no intergroup differences for these categorical variables, neurological deficits were found more frequently in the group A. Dysarthria and pseudobulbar palsy were found exclusively in the group A; these symptoms did not respond to adequate anti-parkinsonian drug treatment, supporting the diagnosis of VaP.

T2-weighted MRI revealed WMLs as well as pontine leukoaraiosis in all patients, while subcortical U fibers were consistently spared (Fig. 1). The mean ± SD number of lacunar infarctions in the striatum was slightly greater in the group A compared with the group B (Table 1: group A, 1.14 ± 0.90; group B, 0.57 ± 0.54; $p = 0.17$). Similarly, the area of lacunae in the striatum was larger in the group A (Table 1; group A, $42.8 \pm 30.3\,mm^2$; group B, $21.7 \pm 21.5\,mm^2$; $p = 0.16$). Consistent with such anatomical changes, FMZ-V_d imaging showed lower values of striatal FMZ-V_d in the group A (Fig. 1).

ROI-based analysis demonstrated that FMZ-V_d tended to be lower in the group A than in the group B (Fig. 2A).

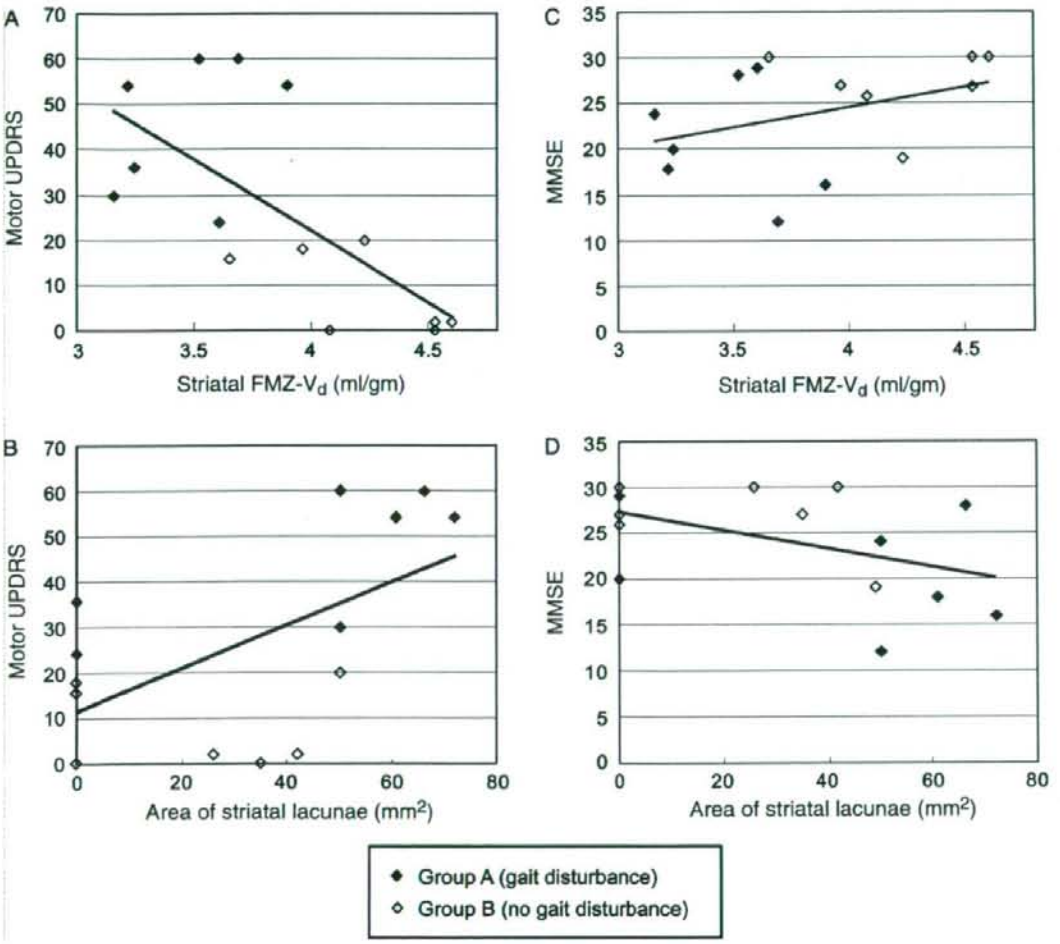

Fig. 4. Correlation of motor UPDRS scores with FMZ-V_d values and infarcted areas in the striatum. (**A**, **B**) The motor UPDRS scores were significantly correlated with the striatal FMZ-V_d values (**A**; r (Pearson) = 0.70; $p < 0.005$) or the striatal infarcted areas (**B**; $r = 0.57$; $p = 0.03$). (**C**, **D**) The MMSE scores were not significantly correlated with the striatal FMZ-V_d values (**C**; $r = 0.35$; $p = 0.21$) or the striatal infarcted areas (**D**; $r = 0.48$; $p = 0.09$). Closed square, patients with gait disturbance (Group A; $n = 7$); open square, patients without gait disturbance (Group B; $n = 7$)

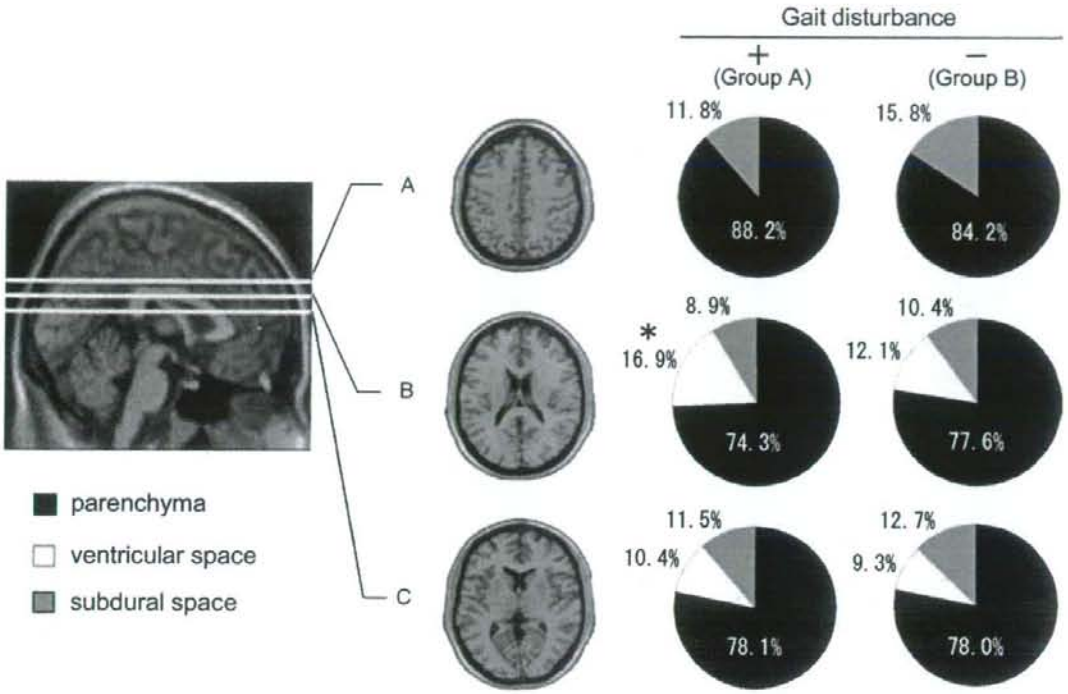

Fig. 5. Comparison of the regional brain volumetry between patients with and without gait disturbance. Brain atrophy was assessed on the three axial slices: immediately superior to the ventricle (**A**), through the body of the ventricle (**B**), and through the anterior and posterior ventricular horns (**C**). Regions occupied by brain parenchyma, subdural space, and ventricular space are indicated as the ratio to total intracranial area at each level. $^{**}p<0.05$

These reductions reached significance in the striatum (17.8%; $p<0.001$), although no significant difference was found in the other areas. The significant difference in the striatal FMZ-V_d still held true after adjusting for differences in MMSE scores by ANCOVA analysis ($p=0.002$). CBF was also reduced in the group A (Fig. 2B), although this reduction only reached significance in the striatum (25.4%; $p<0.05$). $CMRO_2$ also tended to be lower in group A, but these values did not reach statistical significance (Fig. 2C). The largest reduction in $CMRO_2$ was detected in the striatum (25.3%, $p=0.076$). No significant differences were detected in OEF.

SPM analysis showed that FMZ-V_d was significantly reduced in the dorsal striatum bilaterally in the group A ($P_{uncorr}<0.001$; Fig. 3A). The area of reduced FMZ-V_d corresponded to a part of the territory supplied by lateral lenticulostriate arteries (Fig. 3B).

Given the significant reduction of striatal FMZ-V_d in group A patients, we next investigated a possible correlation between striatal FMZ-V_d and parkisonian motor handicap assessed by motor UPDRS. We found a significant inverse correlation of striatal FMZ-V_d with motor UPDRS score (Fig. 4A; $r=0.70$, $p<0.005$). In addition, the area of striatal lacunae positively correlated with the motor UPDRS score (Fig. 4B; $r=0.57$, $p<0.05$); however, the correlation was weaker than that between striatal FMZ-V_d and the motor UPDRS score. The MMSE scores were not significantly correlated with the striatal FMZ-V_d (Fig. 4C; $r=0.035$, $p=0.21$) or with the areas of striatal lacunae (Fig. 4D; $r=0.48$, $p=0.09$).

The regional volumetry showed a significant difference in the area of ventricular bodies, but not in the area of ventricular horns between the groups A and B (Fig. 5).

Discussion

The above results showed that FMZ-V_d and CBF were significantly reduced in the striatum of patients with WMLs who manifested gait disturbance ('lower body' parkinsonism) compared to those who did not. Since FMZ binding reflects neuronal integrity (Heiss et al., 1998; Ihara et al., 2001, 2004) and is relatively unaffected by CBF (Holthoff

et al., 1991), our results suggest that patients with WMLs develop Parkinson-like gait disorders probably due to impaired neuronal integrity in the striatum resulting from ischemia. Consistent with this was the increased number of lacunae in the striatum in our patients with Parkinson-like gait disorders and a previous ^{15}O PET study suggesting that small vessel pathology leads to local ischemic changes in the striatum along with WMLs, jointly contributing to VaP (De Reuck et al., 2001). The lateral lenticulostriate arteries mainly supply the striatum including the putamen (Braffman et al., 1988), and reduced blood flow within several lenticulostriate arteries might impair striatal integrity insidiously. If such striatal flow reduction exceeds a certain threshold and/or spreads to become bilateral, VaP may eventually occur. Given that the striatum plays a pivotal role in correlating the basal ganglia-thalamocortical motor system (higher-order motor control) to the nigrostriatal dopaminergic system (extrapyramidal motor control) (Thompson and Marsden, 1987), chronic ischemic damage to the striatum may well contribute to developing motor impairment such as VaP.

In addition to the 'direct' striatal ischemia, a global loss of neuronal connections may also have affected the neuronal integrity in the striatum because a significant reduction of striatal FMZ-V_d can be interpreted as a group effect across all brain regions. In fact, the ROI-based analysis showed global reductions in FMZ-V_d, rCBF, and $rCMRO_2$ in group A (gait disturbance) patients. Furthermore, the body of the ventricle was significantly dilated in the group A patients, indicative of atrophy and damage of the deep white matter. In such damaged white matter, motor circuits between cortical and subcortical structures, including the basal ganglia-thalamocortical circuit, may be subject to retrograde and/or transsynaptic neuronal degeneration, secondarily disrupting neuronal integrity in the striatum (Brodal, 1981). As is suggested by a previous CT analysis (van Zagten et al., 1998), ischemic damage to the striatum as well as the deep white matter could synergistically disrupt the cortico-subcortical motor circuits, thus contributing to the development of VaP.

To reinforce our interpretation of the results, we should exclude the possibility that the presence of dementia in the group A patients confounded the results because the VaP and vascular dementia are related entities and the mean MMSE score was reduced to 21 points in the group A patients, which is below the cut-off points for dementia. The global reductions in FMZ-V_d, rCBF, and $rCMRO_2$ in group A patients may represent a basis for the reduced MMSE scores. However, the MMSE scores did not correlate with the striatal FMZ-V_d values, and adjustment for differences in MMSE scores did not eliminate the significant difference in the striatal FMZ-V_d between group A and B patients. Furthermore, we found a significant correlation of the motor UPDRS scores with the infarcted areas in the striatum, and more strongly, with the FMZ-V_d values in the striatum. Hence, we conclude that the anatomical as well as functional alterations in the striatum are associated with Parkinson-like gait disorders but not with dementia in patients with WMLs.

In other movement disorders including IPD and progressive supranuclear palsy, the number of striatal BZRs was reported to be within normal limits in postmortem brains using [^{3}H]flunitrazepam *ex vivo* autoradiography (Maloteaux et al., 1998). In addition, FMZ-PET examination in patients with progressive supranuclear palsy and multiple system atrophy demonstrated preservation of BZRs in the striatum (Gilman et al., 1994; Foster et al., 2000). These findings suggest that striatal neuronal integrity is more severely impaired in VaP compared to other movement disorders. The high vulnerability of the striatum in small vessel disease may partially explain the difference (Pantoni et al., 2002).

Certain clarifications need to be addressed regarding the accuracy of the FMZ-V_d. Since the striatal density of BZRs is relatively low, the striatum was reported to exhibit a high variance in B_{max} and K_d values when obtained from FMZ-PET (Abadie et al., 1992). In our study, however, we placed the striatal ROI on the summed FMZ uptake images, and utilized the differences in FMZ uptake among the striatum, the cerebral cortex, and the ventricle. The SEM values were not large in the striatum (see Fig. 2), implying that the determinations of ROIs in the striatum were reliable. Second, significant atrophy could lead to displacement of the striatum and affect our SPM analysis. However, on the axial slice through the striatum and ventricular horns, regions occupied by brain parenchyma, subdural space, and ventricular space were comparable between the two cohorts, thus making unlikely the possibility of striatal displacement. The consistent results between the ROI-based analysis and the SPM analysis further support the accuracy of FMZ-V_d in the striatum.

In conclusion, differences in neuronal integrity in the striatum may determine whether patients with WMLs develop VaP or not. Although the relatively small number of subjects and the absence of neuropathological confirmation are potential limits of this study, the strong correlation between the striatal FMZ-V_d values and the UPDRS scores supports the above conclusion. Thus, the striatal FMZ binding could be a reliable diagnostic marker for VaP. Since therapeutic intervention could be effective in preventing the latent progression of VaP symptoms (Zijlmans et al.,

1995; Winikates and Jankovic, 1999; Foltynie et al., 2002; Sibon et al., 2004), further research is warranted as to how the functional integrity of the striatum can be maintained.

Acknowledgments

This study was supported by a Grant-in-Aid for Japan Society for the Promotion of Science (JSPS) Fellows (M.I.), and also partly supported by Grant-in-Aid for Scientific Research on Priority Areas (B) from JSPS and "Science of Mind" from the Japanese Ministry of Health and Labor (H.F.).

References

Abadie P, Baron JC, Bisserbe JC, Boulenger JP, Rioux P, Travere JM, Barre L, Petit-Taboue MC, Zarifian E (1992) Central benzodiazepine receptors in human brain: estimation of regional Bmax and KD values with positron emission tomography. Eur J Pharmacol 213: 107–115

Bhatia KP, Marsden CD (1994) The behavioural and motor consequences of focal lesions of the basal ganglia in man. Brain 117: 859–876

Braffman BH, Zimmerman RA, Trojanowski JQ, Gonatas NK, Hickey WF, Schlaepfer WW (1988) Brain MR: pathologic correlation with gross and histopathology, 1: lacunar infarction and Virchow Robin spaces. AJR Am J Roentgenol 9: 621–628

Brodal A (1981) Neurological anatomy in relation to clinical medicine, 3rd edn. Oxford University Press, New York

De Reuck J, Siau B, Decoo D, Santens P, Crevits L, Strijckmans K, Lemahieu I (2001) Parkinsonism in patients with vascular dementia: clinical, computed- and positron emission-tomographic findings. Cerebrovasc Dis 11: 51–58

Ebersbach G, Poewe W (2006) Vascular parkinsonian syndrome. Nervenarzt 77: 139–144, 146–147

Foltynie T, Barker R, Brayne C (2002) Vascular parkinsonism: a review of the precision and frequency of the diagnosis. Neuroepidemiology 21: 1–7

Foster NL, Minoshima S, Johanns J, Little R, Heumann ML, Kuhl DE, Gilman S (2000) PET measures of benzodiazepine receptors in progressive supranuclear palsy. Neurology 54: 1768–1773

Frackowiak RS, Lenzi GL, Jones T, Heather JD (1980) Quantitative measurement of regional cerebral blood flow and oxygen metabolism in man using ^{15}O and positron emission tomography: theory, procedure, and normal values. J Comput Assist Tomogr 4: 727–736

Friston KJ, Holmes AP, Worsley KJ, Poline JP, Frith CD, Frackowiak RSJ (1995) Statistical parametric maps in functional imaging: a general linear approach. Hum Brain Mapp 2: 189–210

Gilman S, Koeppe RA, Junck L, Kluin KJ, Lohman M, St Laurent RT (1994) Patterns of cerebral glucose metabolism detected with positron emission tomography differ in multiple system atrophy and olivopontocerebellar atrophy. Ann Neurol 36: 166–175

Heiss WD, Grond M, Thiel A, Ghaemi M, Sobesky J, Rudolf J, Bauer B, Wienhard K (1998) Permanent cortical damage detected by flumazenil positron emission tomography in acute stroke. Stroke 29: 454–461

Holthoff VA, Koeppe RA, Frey KA, Paradise AH, Kuhl DE (1991) Differentiation of radioligand delivery and binding in the brain: validation of a two-compartment model for [^{11}C]flumazenil. J Cereb Blood Flow Metab 11: 745–752

Ihara M, Fukuyama H, Lee T, Takao S, Kohara N, Shibasaki H (2001) Delayed synaptic dysfunction of association cortices in carbon monoxide intoxication. Ann Neurol 50: 829–830

Ihara M, Tomimoto H, Ishizu K, Mukai T, Yoshida H, Sawamoto N, Inoue M, Doi T, Hashikawa K, Konishi J, Shibasaki H, Fukuyama H (2004) Decrease in cortical benzodiazepine receptors in symptomatic patients with leukoaraiosis, a positron emission tomography study. Stroke 35: 942–947

Jellinger KA (2003) How valid is the clinical diagnosis of Parkinson's disease in the community? J Neurol Neurosurg Psychiatry 74: 1005–1006

Lammertsma AA, Jones T (1983) Correction for the presence of intravascular oxygen-15 in the steady-state technique for measuring regional oxygen extraction ratio in the brain: 1. Description of the method. J Cereb Blood Flow Metab 3: 416–424

Magata Y, Mukai T, Ihara M, Nishizawa S, Kitano H, Ishizu K, Saji H, Konishi J (2003) Simple analytical method of ^{11}C-flumazenil metabolite in blood. J Nucl Med 44: 417–421

Maloteaux JM, Luabeya MA, Vanisberg MA, Laterre EC, Laduron PM, Javoy-Agid F, Agid Y (1998) Benzodiazepine receptors in normal human brain, in Parkinson's disease and in progressive supranuclear palsy. Brain Res 446: 321–332

Mikolajczyk K, Szabatin M, Rudnicki P, Grodzki M, Burger C (1998) A JAVA environment for medical image data analysis: initial application for brain PET quantitation. Med Inform (Lond) 23: 207–214

Olsen RW (1981) The GABA postsynaptic membrane receptor-ionophore complex. Site of action of convulsant and anticonvulsant drugs. Mol Cell Biochem 39: 261–279

Pantoni L, Palumbo V, Sarti C (2002) Pathological lesions in vascular dementia. Ann N Y Acad Sci 977: 279–291

Rampello L, Alvano A, Battaglia G, Raffaele R, Vecchio I, Malaguarnera M (2005) Different clinical and evolutional patterns in late idiopathic and vascular parkinsonism. J Neurol 252: 1045–1049

Schmidt R, Hayn M, Fazekas F, Kapeller P, Esterbauer H (1996) Magnetic resonance imaging white matter hyperintensities in clinically normal elderly individuals. Correlations with plasma concentrations of naturally occurring antioxidants. Stroke 27: 2043–2047

Sibon I, Fenelon G, Quinn NP, Tison F (2004) Vascular parkinsonism. J Neurol 251: 513–524

Thompson PD, Marsden CD (1987) Gait disorder of subcortical arteriosclerotic encephalopathy: Binswanger's disease. Mov Disord 2: 1–8

van Zagten M, Lodder J, Kessels F (1998) Gait disorder and parkinsonian signs in patients with stroke related to small deep infarcts and white matter lesions. Mov Disord 13: 89–95

Winikates J, Jankovic J (1999) Clinical correlates of vascular parkinsonism. Arch Neurol 56: 98–102

Yamanouchi H, Nagura H (1997) Neurological signs and frontal white matter lesions in vascular parkinsonism. A clinicopathologic study. Stroke 28: 965–969

Yamauchi H, Fukuyama H, Nagahama Y, Nishizawa S, Konishi J (1999) Uncoupling of oxygen and glucose metabolism in persistent crossed cerebellar diaschisis. Stroke 30: 1424–1428

Zijlmans JC, Thijssen HO, Vogels OJ, Kremer HP, Poels PJ, Schoonderwaldt HC, Merx JL, van 't Hof MA, Thien T, Horstink MW (1995) MRI in patients suspected of vascular parkinsonism. Neurology 45: 2183–2188

European Journal of Neurology 2007, 14: 95–101 doi:10.1111/j.1468-1331.2006.01567.x

Subinsular vascular lesions: an analysis of 119 consecutive autopsied brains

H. Tomimoto[a], J. Lin[a], M. Ihara[a], R. Ohtani[a], A. Matsuo[a] and Y. Miki[b]
Departments of [a]Neurology and [b]Diagnostic Radiology, Graduate School of Medicine, Kyoto University, Sakyo-ku, Kyoto, Japan

Keywords:
autopsied brain, cerebrovascular disease, dementia, insula, white matter,

Received 12 January 2006
Accepted 3 May 2006

The insula of Reil constitutes a functionally intriguing complex of the brain related to multifunctional activities. We examined the subinsular region in 119 consecutively autopsied patients, as T2 hyperintense lesions are frequently observed in magnetic resonance diagnosis of this region. The patients were admitted in neurology wards and were diagnosed as having cerebrovascular disease in 55 patients (46%), other neurological diseases in 57 patients (48%) and non-neurological diseases in seven patients (6%). Demyelination of the white matter was semi-quantified as a fiber density score (percent stained area/total area) with computer-assisted image analysis on Klüver–Barrera-stained sections. Astrogliosis was assessed by immunohistochemistry for glial fibrillary acidic protein. The lesion analysis showed a dilated perivascular space in 29 patients (24%), demyelination (fiber density score less than the mean − 1 SD) in 27 patients (23%), slit-shaped lesion in six patients (5%), lacunar infarction in one patient (1%) and cerebral hemorrhage in one patient (1%). A histologic–radiologic comparison in two patients with subcortical ischemic vascular dementia showed correspondence between subinsular hyperintensities, and demyelination, gliosis and a dilated perivascular space. These results indicate that subinsular lesions rarely signifies focal vascular lesions, and are consisted of demyelination, gliosis and a dilated perivascular space.

Introduction

The insula of Reil is located beneath the frontoparietal and temporal opercula, and covers the basal ganglia, the external capsule, the claustrum and the capsula extrema. It has a diverse connection with the entire cerebral cortex, especially frontoparietal and temporal cortices, the basal ganglia, thalamus and the limbic structures. Therefore, it constitutes a functionally intriguing complex related to multifunctional activities of the brain. These include a pain processing in the human secondary somatosensory area (SII), visceral motor sensory processing and gustatory, vestibular and neuropsychiatric functions. Herein, we use the term of 'subinsular region' to refer to the insular cortex, extreme capsule, claustrum and the external capsule. This region also harbors trajectories passing through it, which include uncinate fasciculus [1], inferior occipitofrontal fasciculus, Meyer's loop [1] and cholinergic projection fibers to the cerebral cortices [2]. This cholinergic projection fibers may be impaired strategically by subinsular lesions in patients with subcortical ischemic vascular dementia (SIVD) [3–5] and cerebral autosomal dominant arteriopathy with subcortical infarcts and leukoencephalopathy (CADASIL) [6].

The subinsular region is vulnerable to ischemic damages, as it is located in the blood flow cliff between the supply from the lateral lenticulostriate arteries and the insular arteries arising from the M3 segment of the middle cerebral artery [7,8]. Therefore, WM lesions in the subinsular region are believed to be ischemic in nature, and continuum of the periventricular WM lesions in the frontal horn. However, little information is available on the neuropathologic substrates corresponding to subinsular hyperintense lesions found on T2-weighted magnetic resonance (MR) images. In CADASIL brains, the correspondents of these lesions are spongiosis and subcortical lacunar lesions in the anterior temporal pole [9], but remain elusive in the subinsular region. In a postmortem MR imaging study of epilepsy patients, Song et al. has addressed subinsular hyperintense lesions to be dilated perivascular spaces [10].

The purpose of the present study is twofold. First, we sought to determine the varieties and frequencies of pathological and non-pathological findings in the subinsular region, as this information can help to understand the nature of the subinsular hyperintense lesions on MR images. Secondly, we compared the premortem radiological findings against the postmortem pathological findings especially in SIVD, and directly determined the pathological nature of subinsular WM lesions, although

Correspondence: Hidekazu Tomimoto, MD, Department of Neurology, Graduate School of Medicine, Kyoto University, Sakyo-ku, Kyoto 606-8507, Japan (tel.: 81 75 751 3766; fax: 81 75 751 3766; e-mail: tomimoto@kuhp.kyoto-u.ac.jp).

premortem radiological films were available only in a limited number of patients.

Subjects and methods

Autopsy specimens

The diagnosis of each patient was based on the combination of pertinent clinical and laboratory findings, and an autopsy examination. We examined 119 brains, including seven from patients who did not have any neurological symptoms or brain lesions (non-neurological control group), 55 from patients with cerebrovascular disease (the CVD group) and 57 from patients with other neurological diseases (the OND group). These patients were autopsied from January 1993 to December 2001 in our institution and its affiliated hospitals which are treating community-dwelling population in the urban area of Kyoto Prefecture. Seven patients had both CVD and ONDs, and they were classified to the OND group. Out of the 119 patients, there were three patients with SIVD, in which clinical and radiologic findings met all of the clinical criteria proposed by Bennett et al. [11]. All patients had a record on radiologic information based on either of computed tomographic (CT) or MR images. Premortem films were available in six patients with CT, and three with MR images which included one with multiple lacunar infarctions and two with SIVD (No. 58 and 67). Hyperintensities were graded in MR images using the following 4-point scale as described by Fazekas et al. [12]: 0, no lesions present; 1, caps and pencil-thin lining; 2, smooth halo; and 3, irregular hyperintensities extending into the deep white matter. The hyperintensities in the external capsule were graded as 0 if they were absent; 1 if their length was shorter than one-fourth of the external capsule; 2, between one-fourth and a half; and 3, longer than one half. Radiological and neuropathological correlations were summarized in Table 1.

Immunohistochemistry

Standard histological examinations were performed on paraffin sections (6 μm-thick) with Klüver–Barrera staining for the observation of myelinated nerve fibers, and hematoxyline and eosin (H&E) staining. A mouse monoclonal antibody against glial fibrillary acidic protein (GFAP; Dakopatts, Glostrup, Denmark, 0.5 μg/ml) was used in the present study. After incubation with the primary antibody, the sections were treated with a biotinylated anti-mouse antibody (Vector Laboratories, ×200) and an avidin–biotin complex (Vector Laboratories, Burlingame, CA, USA, ×200) in 0.02 M PBS containing 0.3% Triton-X (PBST). The sections were finally incubated in 0.01% diaminobenzidine tetrahydrochloride and 0.005% H_2O_2 in 50 mM Tris–HCl (pH 7.6). To test the specificity of the immunohistochemical reaction, control sections were treated with normal mouse IgG instead of the primary antibody.

Image analysis

The subinsular region was defined as the insular cortex, extreme capsule, claustrum and the external capsule. The severity of demyelination in the external and extreme capsules was semi-quantified as follows. The positive areas above an intensity threshold (set at 60% of the mean pixel values within the outlined area of Klüver–Barrera staining) were digitized on an Apple personal computer (PC7500) with a LS-1000 film scanner (Nikon) at a resolution of 1350 dots per inch. These data were saved as 8-bit gray scale PICT files (256 shades of gray), and were analyzed using the NIH image analyzer program by counting the percentage of positive area as the score for myelinated fiber density (myelinated fiber density score). Each image measured 1060.6 × 757.6 μm and consisted of 1893 × 1197 pixels. The myelinated fiber density score was averaged across three representative rectangles from each of the regions of interest in each patient (Fig. 1; labels 1–3 for the external capsule and 4–6 for the extreme capsule). Subinsular demyelination was judged to be present if the fiber density score was less than the mean − 1 SD of all the fiber density scores in either the external or extreme capsules (39.4% for the former and 42.4% for the latter). In a preliminary experiment with eight brains, reproducibility of the estimation ranged at most a 4% variance [16].

Dilatation of the perivascular space was judged to be present if five to six or more small arteries had a perivascular space with a diameter 1.5 times larger than that of the small arteries. Lacunar infarction denoted a small cavity with a diameter between 3 and 15 mm.

Statistical analysis

The statistical significance of intergroup differences was assessed by a one-factor ANOVA followed by Scheffe's F procedure between each group, using StatView II software (version 5.0, for Macintosh; SAS Institute, Tokyo, Japan).

Results

Amongst the 119 patients, 55 were diagnosed with CVD (46%), 57 with ONDs (48%) and seven with non-neurological diseases (6%) (Table 2). The other neurological patients were consisted of 45 with neurodegenerative

Table 1 Radiological and pathological correlation in each patient

Patient no.	Age/gender	Disease	Radiological findings (Rt/Lt) APV	SI	Pathological findings (Rt/Lt SI) Demyelination	Dilated perivascular space
MRI						
58	86/F	SIVD	3/3	3/3	+/+	+/+
67	82/F	SIVD	3/3	2/3	+/+	+/+
114	54/M	Multiple lacunar infarction	2/2	1/1	−/−	−/−
CT						
28	72/F	Multiple lacunar infarction	+/+	0/0	−/−	−/−
38	84/F	SDAT	−/−	1/1	−/−	+/+
80	86/F	Multiple lacunar infarction	+/+	2/2	+/+	−/−
86	90/F	SDAT	+/+	2/1	+/+	+/+
94	88/F	SDAT	+/+	1/2	−/−	+/+
102	84/F	SDAT	−/−	2/3	+/+	+/+

APV, anterior periventricular region; Rt, right; Lt, left; SI, subinsular region; SIVD, subcortical ischemic vascular dementia; SDAT, senile dementia of Alzheimer type. The scores in the radiological findings were determined as described in the Subjects and methods.

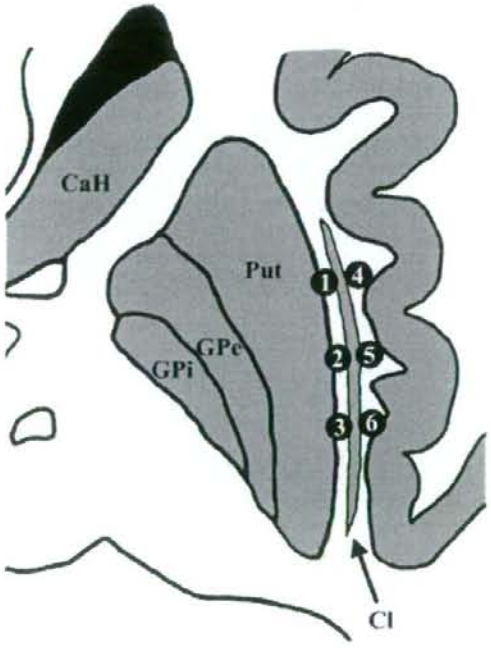

Figure 1 A schematic drawing indicating the region for semi-quantitative image analysis. The labels (1)–(3) indicate for the external capsule and (4)–(6) for the extreme capsule. CaH, caudate head; Put, putamen; GPe, external segment of the globus pallidus; GPi, internal segment of the globus pallidus; Cl, claustrum.

disorders, six with central nervous system infection, three with neuromyopathy, two with brain tumor and one with metabolic encephalopathy. The non-neurological disease patients were consisted of three with pulmonary cancer, one with hepatic cancer, two with pneumonia, and one with rheumatoid arthritis. The mean age in the CVD group was significantly higher than the OND and non-neurological groups. The brain weight was significantly lower in the CVD and OND groups than in the non-neurological control group. Amongst the confounding factors including age, brain weight and myelinated fiber density scores in the external and extreme capsules, a significant correlation was found only between the myelinated fiber density scores of the external and extreme capsules ($R = 0.868$). There were no significant differences in the myelinated fiber density scores between the three groups in both the external and extreme capsules (Table 2), nor any relationships to age ($R = 0.009$ for the external capsule; $R = 0.014$ for the extreme capsule). In the CVD group, however, the myelinated fiber density scores were significantly lower in patients with cerebral hemorrhage than small vessel infarction.

A dilated perivascular space was observed in 29 of 119 patients (24%), more frequently in the CVD and OND groups than in the non-neurological control group (Table 3). In these brains, small arteries with a dilated perivascular space penetrated into the insular cortex, and coursed medio-superiorly in the lower one-third of the extreme capsule (Fig. 2A). On the contrary, the lateral lenticulostriate arteries with a markedly

Table 2 Baseline characteristics and nerve fiber density scores in each group

	Number of patients (male)	Age (years)	Brain weight (g)	Nerve fiber density scores (%)	
				External capsule	Extreme capsule
CVD	55 (29)	77 ± 14*	1151 ± 131	48.6 ± 10.1	51.0 ± 9.3
Cerebral hemorrhage	7 (4)	79 ± 10	1146 ± 170	40.8 ± 11.1**	42.4 ± 11.1**
Small vessel infarction	27 (12)	79 ± 11	1157 ± 127	49.9 ± 9.3	52.9 ± 7.3
Cortical infarction	21 (13)	74 ± 17	1144 ± 132	49.6 ± 10.3	51.4 ± 9.9
OND	57 (30)	66 ± 11	1177 ± 209	48.9 ± 9.0	50.7 ± 8.2
Non-neurological controls	7 (4)	66 ± 11	1252 ± 129	50.8 ± 9.7	53.1 ± 6.9

CVD, cerebrovascular disease; OND, other neurological disease. Small vessel infarction comprises multiple lacunar infarctions and subcortical ischemic vascular dementia.
*Significant at $P < 0.01$ compared with the other two groups. **Significant at $P < 0.05$ compared with the small vessel infarction.

Table 3 Types of lesions amongst the 119 consecutive autopsied brains

Type of lesions	*n* (%)
1. Dilated perivascular space	29 (24)
CVD	15/55
OND	13/57
Non-neurological controls	1/7
2. Demyelination	27 (23)
CVD	15/55
Cerebral hemorrhage	5
Multiple lacunar infarctions	4
SIVD	3
Cortical infarction	2
Hypoxic encephalopathy	1
OND	10/57
Non-neurological controls	2/7
3. Slit-shaped lesion in the lateral edge of the putamen	6 (5)
CVD	4/55
OND	1/57
Non-neurological controls	1/7
4. Lacunar infarction	1 (1)
5. Primary hemorrhage	1 (1)

CVD, cerebrovascular disease; OND, other neurological disease; SIVD, subcortical ischemic vascular dementia. The numbers in parenthesis indicate the percent ratio of the 119 brains. Demyelination was overlaid with a dilated perivascular space in nine brains and with the slit-shaped lesion in one brain.

dilated perivascular space occasionally penetrated into the lower lateral edge of the putamen (Fig. 2B). Subinsular demyelination, with a myelinated fiber density score less than the mean − 1 SD, was observed in 27 of the 119 patients (23%) (Fig. 2C,D). Twelve of the 27 patients were suffering from small vessel disease, including five with hypertensive cerebral hemorrhage, four with multiple lacunar infarctions and three with SIVD (Table 3). The immunohistochemistry for GFAP confirmed that subinsular demyelination was associated with astrogliosis (Fig. 2E,F). Slit-shaped lesions, being different from a lacunar infarction in their shapes, were observed in the lateral edge of the putamen in six patients, in which three suffered from hypoxic encephalopathy (Table 3, data not shown). The subinsular demyelination coexisted with a dilated perivascular space in nine patients, and with a slit-shaped lesion in one patient. Focal lesions were rarely found, only with one patient having a lacunar infarction restricted to the lower end of the extreme capsule and the insular cortex (Fig. 2G), and one patient having a subinsular hemorrhage (Fig. 2H).

A relatively good correlation was found between radiologic–histologic findings in the subinsular region (Table 1). With respect to MR images, linear hyperintense lesions were found in the subinsular region of the two SIVD patients (No. 58 and 67). Patient No. 58 had linear hyperintensities (Fig. 3A,B), whereas those in patient No. 67 were ribbon-like and limited to the anterior half of the subinsular region (Fig. 3C,D). Demyelination in the external capsule was obvious in patient No. 58 when compared with the control patients (Fig. 3E,F), with myelinated fiber density scores of 33.9% for the external capsule. In contrast, patient No. 67 had mild demyelination (Fig. 3G), with myelinated fiber density scores of 37.9% in the external capsule, and had a dilated perivascular space in the subinsular region at the lower putamen level (Fig. 3H). Neither of these two patients had focal lesions such as lacunar infarction or cerebral hemorrhage in the subinsular region.

Discussion

White matter lesions in the external capsules are known to be frequently observed in radiological diagnosis for CADASIL and SIVD [9,13–16]. The present study further revealed that subinsular WM lesions correspond pathologically to demyelination and gliosis at the mid-putamen level, and a dilated perivascular space at the lower putamen level in SIVD. These neuropathological substrates for WM lesions were observed not only in the CVD group but also in

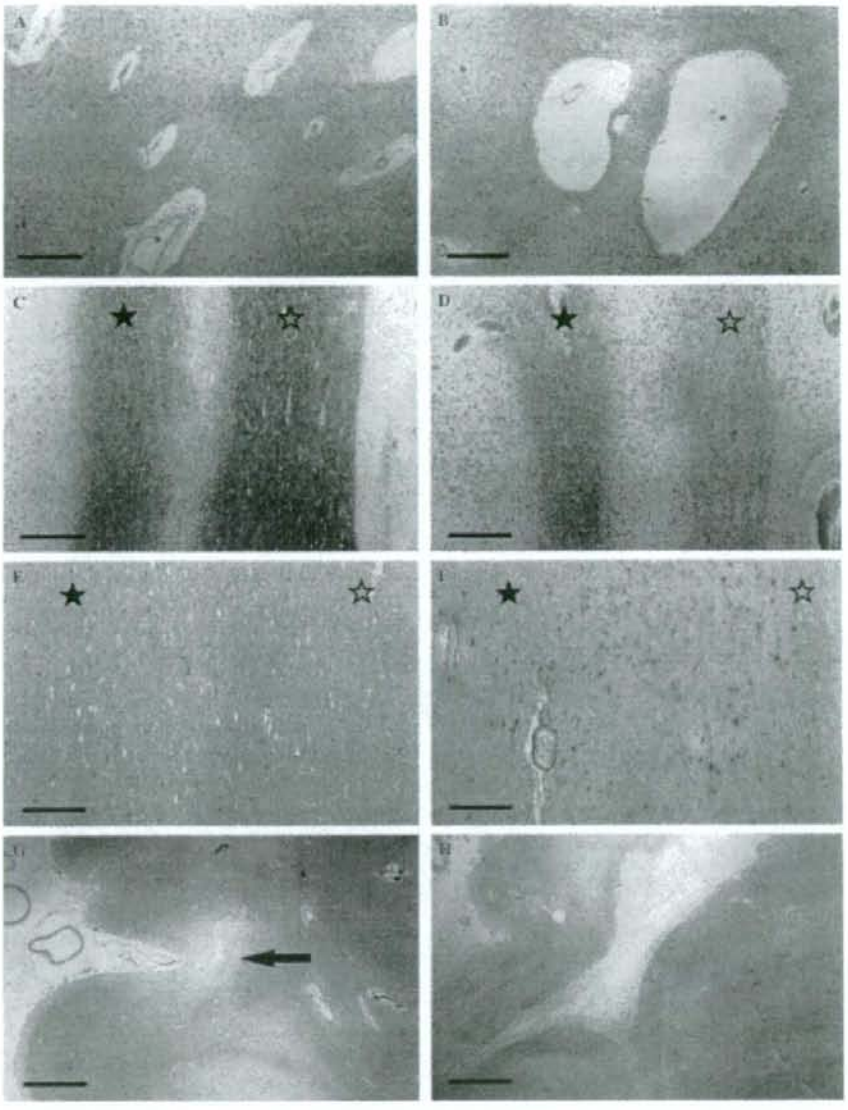

Figure 2 Photomicrographs of the H&E staining (A, B, G, H), Klüver–Barrera staining (C, D) and immunohistochemistry for GFAP (E, F). A dilated perivascular space in the lower one-third of the extreme capsule (A); a lateral lenticulostriate artery with a dilated perivascular space turns dorsally at the lower lateral edge of the putamen (B); demyelination (D) and astrogliosis (F) is observed in patient No. 67 when compared with a control subject (C, E); lacunar infarction at the lower end of the extreme capsule and insular cortex (G); and old subinsular hemorrhage (H). The filled asterisks indicate the extreme capsule and open asterisks indicate the external capsule (C–F). Bars indicate 500 μm (A–D), 200 μm (E, F) and 2 mm (G, H).

the OND and non-neurological control groups in the consecutive autopsy brains. A significantly higher age in the CVD group may have strengthened these WM lesions, as WM lesions are known to be strongly associated with aging. The neuropathological changes were common to those seen in the periventricular

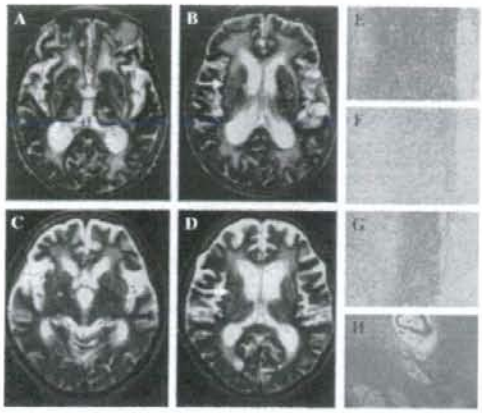

Figure 3. MR images of SIVD patients (A and B from patient No. 58, C and D from patient No. 67) and photomicrographs of Klüver–Barrera staining in the external capsule (E from a control subject, F from patient No. 58, G from patient No. 67) and H&E staining in the lower lateral edge of the putamen (H from patient No. 67). The arrows in (B) and (D) indicate the corresponding regions in (F) and (G), respectively. Note that the subinsular hyperintensities are severe in (A, B) and mild in (C, D). Patient No. 58 had obvious demyelination (F) when compared with the control (E), whereas in patient No. 67, the demyelination was mild (G) with a dilated perivascular space in the subinsular region at the lower putamen level (H).

WM, supplementing the notion that subinsular WM lesions are continuum of the periventricular WM lesions in a previous CT study [17].

Demyelination and gliosis of the WM can be experimentally induced by chronic cerebral hypoperfusion in rodents, supplementing that this type of WM lesions are caused by chronic cerebral ischemia [18–20]. In addition, cerebral edema may be another causative mechanism leading to WM lesions. Extravasated edema fluid is transported into the vascular systems in the periventricular WM, and is finally drained into the ventricular CSF. Thus, subinsular WM lesions may be pathogenetically attributable to chronic cerebral ischemia and/or cerebral edema.

In previous studies, another types of lesions except for demyelination and gliosis have been also reported in the subinsular region. A postmortem MR imaging study revealed that subinsular hyperintensities corresponded to dilated perivascular spaces in the lower portion of the extreme capsule [10]. Furthermore, a single dilated perivascular space appeared as a large hyperintense spot in the lower lateral edge of the putamen [21,22]. In concordance with these results, the dilated perivascular space was found in the lower one-third of the extreme capsule and the lower lateral edge of the putamen. The insular arteries penetrate and course medio-superiorly toward the claustrum in the lower one-third of the extreme capsule. On the contrary, the lateral lenticulostriate arteries penetrate and turn dorsally in the lower lateral edge of the putamen. Dilated perivascular space is reported to show punctate hyperintensities, whereas demyelination is more likely to correspond to extensive ill-defined lesions [23].

Thus, the present study demonstrated two types of subinsular lesions: demyelination and gliosis extending from the anterior periventricular WM lesions at the mid-putamen level; and dilated perivascular spaces at the lower putamen level. In clinical practice, insular stroke restricted to the insular cortex is exceptional [24]. The present series also included only one patient with either subinsular lacunar infarction or hemorrhage, indicating that a focal lesion is extremely rare in this region. Although the radiological features of subinsular lacunar infarction remain unclear, it is expected that subinsular hyperintensities most likely reflect demyelination, gliosis and a dilated perivascular space from the viewpoint of the frequency of these neuropathological substrates.

In conclusion, subinsular T2 hyperintensities rarely correspond to lacunar infarction or cerebral hemorrhage, but correspond to demyelination and gliosis at the mid-putamen level, and dilated perivascular spaces at the lower putamen level.

Acknowledgments

This work was supported by grants from the Ministry of Education, Culture, Sports, Science and Technology, Japan (H. T.). We are indebted to Miss Hitomi Nakabayashi for her excellent technical assistance.

References

1. Kier EL, Staib LH, Davis LM, Bronen RA. MR Imaging of the temporal stem: anatomic dissection tractography of the uncinate fasciculus, inferior occipitofrontal fasciculus, and Meyer's loop of the optic radiation. *American Journal of Neuroradiology* 2004; **25:** 677–691.
2. Selden NR, Gitelman DR, Salamon-Murayama N, Parrish TB, Mesulam MM. Trajectories of cholinergic pathways within the cerebral hemispheres of the human brain. *Brain* 1998; **121:** 2249–2257.
3. Wallin A, Alafuzoff I, Carlsson A, *et al.* Neurotransmitter deficits in a non-multi-infarct category of vascular dementia. *Acta Neurologica Scandinavica* 1989; **79:** 397–406.
4. Swartz RH, Sahlas DJ, Black SE. Strategic involvement of cholinergic pathways and executive dysfunction: does location of white matter signal hyperintensities matter? *Journal of Stroke and Cerebrovascular Disease* 2003; **12:** 29–36.
5. Tomimoto H, Ohtani R, Shibata M, Nakamura N, Ihara M. Loss of cholinergic pathway in vascular dementia of

the Binswanger type. *Dementia Geriatric Cognitive Disorders* 2005; **19:** 282–288.
6. Mesulam M, Siddique T, Cohen B. Cholinergic denervation in a pure multi-infarct state: observations on CADASIL. *Neurology* 2003; **60:** 1183–1185.
7. Marinkovic R, Markovic L. The role of the middle cerebral artery in the vascularization of the claustrum. *Medicinski Pregled* 1990; **43:** 361–365.
8. Ture U, Yasargil MG, Al-Mefty O, Yasargil DC. Arteries of the insula. *Journal of Neurosurgery* 2000; **92:** 676–687.
9. van Den Boom R, Lesnik Oberstein SA, van Duinen SG, *et al.* Subcortical lacunar lesions: an MR imaging finding in patients with cerebral autosomal dominant arteriopathy with subcortical infarcts and leukoencephalopathy. *Radiology* 2002; **224:** 791–796.
10. Song CJ, Kim JH, Kier EL, Bronen RA. MR imaging and histologic features of subinsular bright spots on T2-weighted MR images: Virchow-Robin spaces of the extreme capsule and insular cortex. *Radiology* 2000; **214:** 671–677.
11. Bennett DA, Wilson RS, Gilley DW, Fox JH. Clinical diagnosis of Binswanger's disease. *Journal of Neurology, Neurosurgery and Psychiatry* 1990; **53:** 961–965.
12. Fazekas F, Kleinert R, Offenbacher H, *et al.* The morphologic correlate of incidental punctate white matter hyperintensities on MR images. *American Journal of Neuroradiology* 1991; **12:** 915–921.
13. Auer DP, Putz B, Gossl C, *et al.* Differential lesion patterns in CADASIL and sporadic subcortical arteriosclerotic encephalopathy: MR imaging study with statistical parametric group comparison. *Radiology* 2001; **218:** 443–451.
14. O'Sullivan M, Jarosz JM, Martin RJ, *et al.* MRI hyperintensities of the temporal lobe and external capsule in patients with CADASIL. *Neurology* 2001; **56:** 628–634.
15. Markus HS, Martin RJ, Simpson MA, *et al.* Diagnostic strategies in CADASIL. *Neurology* 2002; **59:** 1134–1138.
16. Tomimoto H, Ohtani R, Wakita H, *et al.* Small artery dementia in Japan; radiological differences between CADASIL, leukoaraiosis and Binswanger's disease. *Dementia Geriatric Cognitive Disorders* 2006; **21:** 162–169.
17. Cobb SR, Mehringer CM, Itabashi HH, Pribram H. CT of subinsular infarction and ischemia. *American Journal of Neuroradiology* 1987; **8:** 221–227.
18. Shibata M, Ohtani R, Ihara M, Tomimoto H. White matter lesions and glial activation in a novel mouse model of chronic cerebral hypoperfusion. *Stroke* 2004; **35:** 2598–2603.
19. Wakita H, Tomimoto H, Akiguchi I, Kimura J. Glial activation and white matter changes in the rat brain induced by chronic cerebral hypoperfusion: an immunohistochemical study. *Acta Neuropathologica (Berlin)* 1994; **87:** 484–492.
20. Roman GC. Brain hypoperfusion: a critical factor in vascular dementia. *Neurology Research* 2004; **26:** 454–458.
21. Poirier J. Giant cerebral lacuna due to dilatation of the perivascular space: a case report. *Clinical Neuropathology* 1983; **2:** 138–140.
22. Pullicino PM, Miller LL, Alexandrov AV, Ostrow PT. Infraputaminal 'lacunes'. Clinical and pathological correlations. *Stroke* 1995; **26:** 1598–1602.
23. Munoz DG, Hastak SM, Harper B, Lee D, Hachinski VC. Pathologic correlates of increased signals of the centrum ovale on magnetic resonance imaging. *Archives of Neurology* 1993; **50:** 492–497.
24. Cereda C, Ghika J, Maeder P, Bogousslavsky J. Strokes restricted to the insular cortex. *Neurology* 2002; **59:** 1950–1955.

Matrix Metalloproteinase-2 Plays a Critical Role in the Pathogenesis of White Matter Lesions After Chronic Cerebral Hypoperfusion in Rodents

Kayoko Nakaji, MD; Masafumi Ihara, MD; Chiaki Takahashi, MD; Shigeyoshi Itohara, PhD; Makoto Noda, PhD; Ryosuke Takahashi, MD; Hidekazu Tomimoto, MD

Background and Purpose—Cerebrovascular white matter (WM) lesions contribute to cognitive impairment and motor dysfunction in the elderly. A disruption of the blood–brain barrier (BBB) is believed to be a critical early event leading to these WM lesions. Previous studies have suggested the involvement of matrix metalloproteinase-2 (MMP-2) in BBB disruptions and the upregulation of MMP-2 after chronic cerebral hypoperfusion in a rat model. In the present study, we asked whether MMP-2 is involved in the BBB disruption and the subsequent WM lesions after chronic cerebral hypoperfusion.

Methods—We compared the severity of white matter lesions in rats after chronic cerebral hypoperfusion with or without an MMP inhibitor. Then, we also induced the chronic cerebral hypoperfusion in wild-type and MMP-2-null mice.

Results—In the rats treated with a relatively selective MMP-2 inhibitor, AG3340, the WM lesions after chronic cerebral hypoperfusion were significantly less severe, and the number of activated astroglia and microglia were also significantly lower as compared with the vehicle-treated rats. Gene knockout of MMP-2 also reduced the severity of the WM lesions and the number of activated astroglia and microglia in a mice system. In both rodents, the disruption of BBB function, as assessed by IgM staining and the Evans blue extravasation test, was less severe when MMP-2 activity was attenuated.

Conclusions—These findings indicate that MMP-2 plays a critical role in the BBB disruption, glial cell activation, and WM lesions after chronic cerebral hypoperfusion and suggest the potential value of MMP-2 inhibitors as a therapeutic tool in cerebrovascular WM lesions. **(*Stroke*. 2006;37:2816-2823.)**

Key Words: blood–brain barrier ■ chronic cerebral hypoperfusion ■ MMP inhibitor ■ MMP-2 ■ white matter lesion

Cerebrovascular white matter (WM) lesions, a neurodegenerative condition characterized by hyperintense signals on magnetic resonance images, are frequently associated with aging and cerebrovascular disease and are responsible for the cognitive decline of the elderly. Chronic cerebral ischemia is likely to cause these WM lesions, because cerebral blood flow is decreased in these patients.[1] Indeed, similar WM lesions can be induced in rats and mice after chronic cerebral hypoperfusion, the experimental conditions mimicking chronic cerebral ischemia in humans.[2,3]

Matrix metalloproteinases (MMPs) are a family of endopeptidases that can degrade most of the major constituents of the extracellular matrix.[4] MMP-2 and MMP-9 represent a subgroup of the MMP family and degrade several extracellular matrix components, including type IV collagen, fibronectin, and gelatin. Deregulated MMPs have been implicated in the tissue destruction associated with cancer, arthritis, and multiple sclerosis.[4] MMPs may also play a role in neurologic disorders. For instance, MMP-9 is increased in human brains after stroke,[5] and MMP-2 and MMP-3 are increased in cerebrovascular WM lesions from patients with vascular dementia.[6] A reduction in the basement membrane components, including type IV collagen, is associated with the blood–brain barrier (BBB) disruption during cerebral ischemia.[7] In our previous study on chronic cerebral hypoperfusion, the BBB disruption was accompanied by an upregulation of MMP-2 but not MMP-9,[8] suggesting the specific involvement of MMP-2 in the WM lesions. We hypothesize that the MMP-2 upregulation after chronic cerebral hypoperfusion correlates with BBB damage, which leads to glial activation and subsequent WM lesions. To clarify the cause–effect relationship among MMP-2 upregulation, BBB disruption, and WM lesions, we used 2 strategies to attenuate MMP-2 activity: an MMP inhibitor, AG3340, and MMP-2

Received March 2, 2006; final revision received June 9, 2006; accepted July 24, 2006.

From the Department of Neurology (K.N., M.I., R.T., H.T.), Horizontal Medical Research Organization (M.I.), the Department of Molecular Oncology (M.N.), and The 21st Century Center of Excellence Program, Department of Oncology (C.T.), Kyoto University Graduate School of Medicine, Kyoto, Japan; and the Laboratory for Behavioral Genetics (S.I.), RIKEN Brain Science Institute, Wako, Japan.

Correspondence to Kayoko Nakaji, MD, Department of Neurology, Graduate School of Medicine, Kyoto University, 54 Kawaharamachi, Shogoin, Sakyo-ku, Kyoto 606-8507, Japan. E-mail kann@kuhp.kyoto-u.ac.jp

Stroke **is available at http://www.strokeaha.org** **DOI: 10.1161/01.STR.0000244808.17972.55**